POLARIMETRIC DOPPLER WEATHER RADAR

R J Doviak, National Severe Storms Laboratory, Norman, Oklahoma, USA

R D Palmer, School of Meteorology, Atmospheric Radar Research Center, University of Oklahoma, USA

Introduction

The term 'Doppler' is in honor of the Austrian physicist, Christian Johann Doppler, who first explained the principle of the 'Doppler effect' in 1842. The Doppler effect is the increase or decrease in the pitch or frequency of sound waves when a source of waves is moving toward or away from the listener. This is quite evident to an observer who is listening to the blare of an automobile horn as it passes by. The observer hears first a relatively high frequency wave and then a marked drop in frequency.

Electromagnetic waves (e.g., light and radio waves) emitted from galaxies also have Doppler shifts. Spectral lines of emitted radiation are Doppler shifted to lower frequencies because most galaxies are moving away in our expanding universe; blue spectral lines are shifted to lower frequency red lines, the so-called 'red shift'.

Unlike sound waves, which have vibrations in the direction of propagation, electromagnetic waves have vibrations in a plane transverse to the direction of propagation. Through careful design of the radar, the direction of the electric field in the plane of oscillation can be controlled thereby creating a particular *polarization*. The polarization of the electromagnetic waves has a profound effect on their interaction with atmospheric scatterers

(e.g., hydrometeors, insects, refractive index perturbations, etc.).

Doppler weather radars owe their acceptance by the weather services around the world to the fact that radio waves having wavelengths on the order of centimeters can penetrate extensive fields of precipitation (e.g., hurricanes) to map and reveal, like an X-ray photograph, the internal structure and motion of weather systems. Optical and infrared waves do not penetrate very far into clouds and precipitation.

How radar uses the Doppler effect to measure the radial velocity of scatterers in the earth's atmosphere, and how measurements of the polarimetric properties of radiation backscattered from these scatterers can be used to improve estimates of rainfall and to distinguish various types of hydrometeors (e.g., rain, snow, hail, etc.) is explained in this article. In the section 'Fundamentals of Polarimetric Doppler Radar', the basic theory of weather radar is provided, including both Doppler and polarimetric measurements. Following this section, examples of Polarimetric and Doppler data are shown to emphasize the usefulness of these measurements to observations of weather. Finally, the authors' perspective on the future of weather radar is provided.

The Doppler Shift and Polarimetric Properties of Scatterers

Scatterers in the atmosphere produce measureable Doppler shifts if the scatterers are illuminated with narrow band radiation (e.g., a radio wave transmitted at a single frequency f_t). Radio waves incident on a scatterer forces electromagnetic vibrations in the scatterer. If the scatterer is at constant range *r* from the transmitter (e.g., radar), vibrations are at f_t. If the scatterer moves

toward the radar, the internal vibrations will be faster because the wave's apparent propagation speed relative to the scatter is faster and thus the approaching scatterer experiences more rapid fluctuations of the incident waves. Thus the backscattered radiation (i.e., echoes) received by the radar will have a frequency higher than f_t.

Doppler weather radars typically transmit microwave radiation in bursts of short duration τ_t (e.g., 10^{-6} seconds or 1 μs). These radars are called pulsed-Doppler radars to distinguish them from those that emit continuous waves (e.g., radars used by police to detect the speed of automobiles). Pulsed-Doppler radars can measure both range r and radial velocity v_r of scatterers.

For example, the USA National Weather Service (NWS) network of Doppler weather radars emit 1.57 μs duration pulses of 10-cm wavelength $\lambda = c / f_t$ radiation (i.e., similar to the λ used in microwave ovens; c is the speed of light) to map r and v_r of hydrometeors. These radars are called WSR-88Ds, where WSR is an acronym of Weather Surveillance Radar. The number 88 denotes the initial year of deployment of the network in 1988, and the letter D represents its Doppler capability.

The measurement of the Doppler shift in a single backscattered pulse (i.e., an echo) of microwaves is not practical. Instead the change of the echo's phase angle from one transmitted pulse to the next is measured as will be describe later in more detail. Phase angle is proportional to the scatterer's range and equals twice the number of wavelengths (and portions thereof) between the radar and the scatterer. Phase angle measures quite precisely (i.e., to fractions of a wavelength) the distance to the scatterer, but there is ambiguity because the phase can be only determined within a wavelength. Nevertheless, the change of the echo phase, from pulse to pulse,

is used to measure v_r, the time rate-of-change of range to the scatterer.

If all hydrometeors were spherical, polarization would not play a major role in the design of weather radar. In stark contrast, hydrometeors can be found in a variety of shapes, sizes, orientations, and size distributions. Simple visual observations of snow, for example, exemplify the vast array of possibilities. Even raindrops, which are often thought to be spherical, exhibit deformation due to drag force. This effect becomes gradually more important with increasing drop size, as illustrated in Figure 1 (note that liquid cloud droplets with diameters on the order of microns are nearly spherical and thus equally backscatter linearly polarized waves of any orientation—e.g., horizontal H or vertical V polarization). The equivalent diameter D_e is the diameter of a spherical drop, which would have the same volume as the deformed drops shown in the figure. Also shown in the figure is the so-called *differential reflectivity* Z_{DR} (a measure of the ratio of backscatter from H and V polarized waves; to be discussed more fully later.).

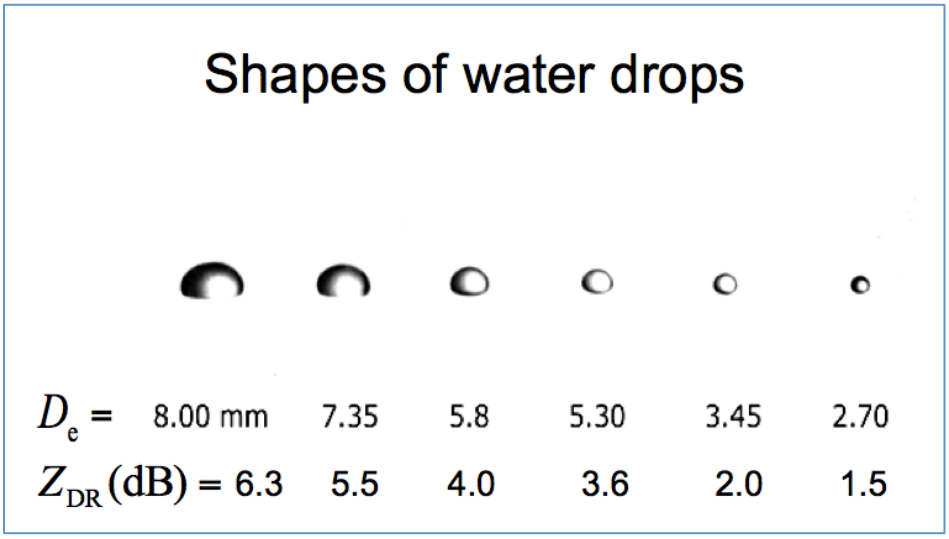

Figure 1 Shapes of raindrops falling in still air and experiencing drag force deformation. D_e is the equivalent diameter of a spherical drop. Z_{DR} (dB) is the differential reflectivity in decibels

for each drop at a radar wavelength of 10 cm. Adapted from Pruppacher and Beard (1970).

It is interesting to note that other types of non-hydrometeorological scatterers found in the atmosphere (e.g., refractivity index perturbations, insects, birds) can also be non-spherical. For these reasons, polarimetric signatures of scatterers are important for weather radar design and can be used for more precise characterization of their properties, leading to accurate rainfall estimates and the capability of hydrometeor classification (i.e., distinguishing rain, snow, hail, etc.).

The most common type of polarimetric weather radar design produces electromagnetic oscillations in a plane (the plane of polarization) orthogonal to the direction of wave propagation. In this plane the electric field vector can be decomposed into two components having orthogonal directions, H and V, the horizontally and "vertically" polarized components. For H polarization the vibrations are parallel with the ground, but for the V polarizations the vibrations lie in a vertical "plane" as illustrated in Figure 2. Due to the non-spherical shape of most hydrometeors, the backscattered signals from each of these linear polarizations will be different. Quantification of these differences is the foundation of polarimetric radar.

H and V linear polarization is often accomplished using a simultaneous-transmit simultaneous-receive (STSR) configuration, as illustrated in Figure 2. As the name implies, electromagnetic waves with both H and V polarizations are transmitted simultaneously. In the STSR mode, the backscattered radiation from the scatterers is also received simultaneously in H and V receivers. Another design alternates from pulse-to-pulse the H, V transmissions, but has simultaneous H and V reception (ATSR). The major advantage of the ATSR configuration is

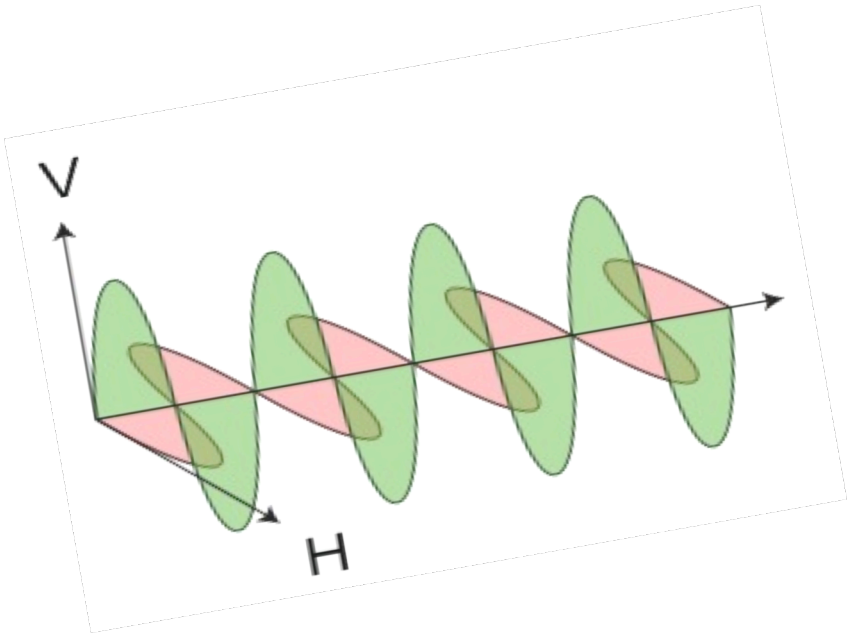

Figure 2 Electromagnetic waves propagating with two orthogonal linear polarizations, which for this case are aligned in time (i.e., *in-phase*). When two waves with H and V polarizations are simultaneously transmitted in-phase, the resulting composite electromagnetic field oscillates along a 45^{o} angle (called *slant linear-45*) in the plane of polarization.

its capability to measure *cross-polar* signals, where backscatter from a horizontally polarized transmitted pulse is received with vertical polarization, for example. Such cross-polar measurements do contain important meteorological information but are extremely weak compared to the *copolar* signals (e.g., horizontally polarized echoes are received when horizontally polarized pulses are transmitted). Implementation challenges of the ATSR mode with high-powered transmitters contributed to the decision by the NWS to use the STSR design for the nascent polarimetric upgrade to the WSR-88D network (Doviak et al. 2000). It should be noted that the ATSR is more applicable to polarimetric phased array radars with distributed, low-powered solid-state transmitters (See the section on Future Weather Radar).

Consider a single stationary hydrometeor at range *r*. The effects on the polarimetric signature can be divided into two components: *propagation effects* and *backscattering effects*. If no precipitation exists between the radar and the hydrometeor, propagation effects can be ignored and any polarimetric signature would be due solely to backscattering effects. For clarity, we will assume this situation. In this case, the backscattered electric field is described by the following matrix equation

$$\begin{bmatrix} E_{\mathrm{h}} \\ E_{\mathrm{v}} \end{bmatrix}^{b} = \begin{bmatrix} s_{\mathrm{hh}} s_{\mathrm{hv}} \\ s_{\mathrm{vh}} s_{\mathrm{vv}} \end{bmatrix} \begin{bmatrix} E_{\mathrm{h}} \\ E_{\mathrm{v}} \end{bmatrix}^{i} \frac{\exp(-jkr)}{r} \tag{1}$$

where $E_{\mathrm{h}}, E_{\mathrm{v}}$ are the electric field components in the h, v direction, the superscripts *i* and *b* correspond to the incident and backscattered fields, respectively, $j = \sqrt{-1}$, and s_{hv} is the complex backscattering matrix element corresponding to vertical transmission and horizontal reception. The other elements of the backscattering matrix follow accordingly. s_{hv} is called complex because it has magnitude (proportional to the size, shape, and orientation of the scatterer) and phase (e.g., the exponent of the exponential factor in the equation is also a phase term). The magnitudes and phases fluctuate in time because the hydrometeor's size, shape, and orientation change due to turbulence and collisions. By independently transmitting and receiving horizontal and vertical polarizations (e.g., ATSR mode), it is possible to measure all the elements of the backscattering matrix, although the cross-polar terms (s_{hv} and s_{vh}) are one to two orders of magnitude weaker than the copolar terms (s_{hh} and s_{vv}). In contrast, the STSR mode allows relatively easy measurement of only the *copolar* terms (s_{hh} and s_{vv}), whereas sophisticated coding schemes (Chandrasekar and Bharadwaj 2009) are required to estimate s_{hv}.

Fundamentals of Polarimetric Doppler Radar

The fundamentals of Polarimetric Doppler radar can be more easily explained by discussing a simplified block diagram of polarimetric homodyne radar (Figure 3). Weather radar has an oscillator (the STALO, an acronym for Stabilized Local Oscillator), which generates a very pure continuous microwave (i.e., a spectral line) at a frequency f_t; this continuous wave is converted to a sequence of microwave pulses by the modulator. Frequency f_t is called the carrier frequency because it carries the modulation pulse. The transmitted microwave pulses, of time duration τ_t

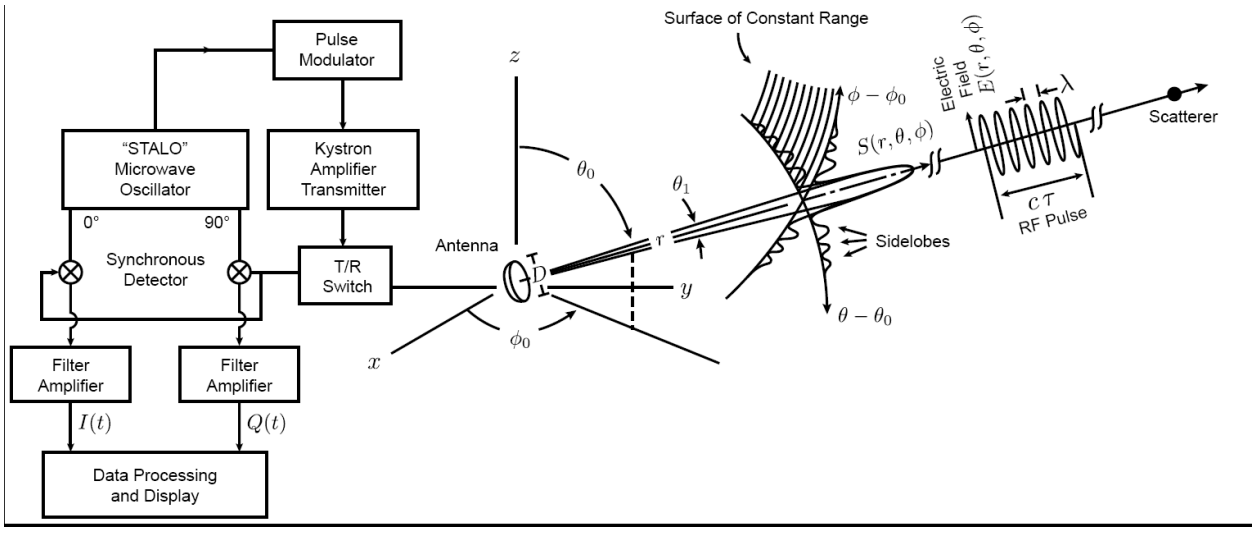

Figure 3 Block diagram for a single V channel (i.e., waves polarized in a vertical plane are transmitted) of a homodyne polarimetric Doppler radar. For STSR mode, the transmitted pulse would be split between H (not shown here) and V channels after the klystron amplifier transmitter and sent to two transmit/receive T/R switches and a dual-polarimetric antenna. Upon receive, the H and V channels would have separate electronics to receive the signals independently.

and spaced T_s ($\simeq 1$ millisecond) are intensified by a high power amplifier (e.g., a klystron) to produce very large peak pulse power P_t, often close to 1 megawatt. The average power $P_{av} = (\tau_t / T_s)P_t$, however, is typically a kilowatt or less, about that used in microwave ovens. The transmitted pulse of vertically polarized microwaves of spatial length $c\tau_t$ is in a beam, formed by the parabolic reflector antenna, directed at azimuth and elevation angles $\cdot\cdot$ = 90°- $\cdot\cdot_0$ and $\theta_e = \frac{\pi}{2} - \theta_0$ respectively (radar meteorologists measure azimuth $\cdot\cdot$ clockwise from North). Weather radar beams typically have a circular half-power angular width $\theta_1 \cong 1^\circ$. It should be recognized that the reflector antenna, which determines the overall quality of the polarimetric signals, is the key component of the radar system. A feed is placed at the focal point of the parabolic reflector and emits the H and V electromagnetic energy onto the reflector.

It is difficult to make direct measurements of the microwave signal, so most receivers shift f_t either to zero as done by a homodyne receiver (Figure 3) or, more commonly, to an intermediate frequency so that the signal can be digitized and analyzed with computers. In a homodyne receiver the echo of pulsed microwaves is directly passed to a synchronous detector (Figure 3) and mixed (multiplied) with signals from the STALO. A synchronous detector is required to resolve both the echo's magnitude and sign of its phase angle or Doppler shift. The two STALO signals are sinusoid and co-sinusoid, producing the *in-phase* and *quadrature* signals, respectively. With advances in digital technology, modern receivers that digitize the signals at the received frequency f_t (or at its shifted intermediate frequency) and translate these signals to baseband (i.e., f_t = 0) are becoming ubiquitous. These so-called *digital receivers*,

or *software-defined receivers*, have several advantages including a perfect quadrature relation between the in-phase and quadrature signals, and a flexible design. Since the receiver characteristics are controlled in software, updates can easily be incorporated as advances in signal processing become operational.

How the pulse-to-pulse shift in echo phase is related to v_r is now explained. We will begin with the simple case of a stationary scatterer at *r*, and will later show how the phase changes when the scatterer is allowed to move. In this case, the copolar echo voltage (e.g., V_{hh}) at the receiver's input is essentially a scaled replica of the transmitted pulse and is given by

$$V_{hh}(r,t) = As_{hh} \exp\left\{j\left[2\pi f_t\left(t - \tfrac{2r}{c}\right) + \psi\right]\right\} U\left(t - \tfrac{2r}{c}\right) \quad (2a)$$

$$= As_{hh}\left[\cos\left(2\pi f_t t - \tfrac{4\pi r}{\lambda} + \psi\right) + j\sin\left(2\pi f_t t - \tfrac{4\pi r}{\lambda} + \psi\right)\right] U\left(t - \tfrac{2r}{c}\right) \quad (2b)$$

The cosine and sine terms are the real and imaginary components of $V_{hh}(r,t)$ oscillating at the rate f_t, A is the echo amplitude, s_{hh} is the copolar backscattering element for HH polarization, $2\pi f_t(t - 2r/c) + \psi$ is the echo phase, t is time the echo is received after the emission of the transmitted pulse, and ψ is the sum of phase shifts within the radar and the scatterer. The pulse function $U\left(t - \dfrac{2r}{c}\right)$ is unity when its argument $t - \dfrac{2r}{c}$ is between 0 and τ_t, and is zero otherwise. The first equation is an exponential form and a compact way of expressing the echo's amplitude and phase.

As just discussed, it is difficult to process the echo voltage at the transmitted microwave frequency f_t so the signal is down-converted to baseband (i.e., zero carrier frequency) using

the synchronous detector (or digital receiver). An expression for this baseband signal can be obtained from equation (2b) by setting $f_t = 0$. Thus, the echo voltage at the receiver's output (HH polarization, in this case) is

$$V_{\mathrm{hh}}(r,t) = I_{\mathrm{hh}}(r,t) + jQ_{\mathrm{hh}}(r,t) \ , \tag{3a}$$

where

$$I_{\mathrm{hh}}(r,t) = As_{\mathrm{hh}} \cos\psi_e \, U\left(t - \tfrac{2r}{c}\right), \tag{3a}$$

$$Q_{\mathrm{hh}}(r,t) = As_{\mathrm{hh}} \sin\psi_e \, U\left(t - \tfrac{2r}{c}\right) \ , \tag{3b}$$

are the in-phase and quadrature components, and the echo phase is defined as

$$\psi_e = -\tfrac{4\pi r}{\lambda} + \psi \tag{4}$$

For simplicity, henceforth the polarimetric notation subscript on the in-phase and quadrature signals is dropped and will be used only where necessary for clarity.

Sampling in Range and Time

As denoted in equation (3), the echo voltage is a function of both range r and time t. Because pulses are transmitted every T_s, echoes from a stationary scatterer will periodically appear at $t = \dfrac{2r}{c} + mT_s$ where m = 1, 2, 3, etc. defines each echo pulse. Because the scatterer's range is not known, a search for echoes is made by circuits that sample, at rates typically > τ_t^{-1}, for echoes and the sampling process is reset every T_s. The T_s interval is defined as *range-time* τ_s $(0 \le \tau_s \le T_s)$ because the location of the echo within T_s defines the range r to the scatterer.

If the scatterer moves, not only will the echo pulse change its location along τ_s, but ψ_e will also change according to (4). Both echo position along τ_s and ψ_e can in principle be used to measure the change in scatterer location, and thus indirectly its radial velocity. However, ψ_e change is a more accurate measure of changes in scatterer location. For example, a change of *r* by $\lambda/4$ (e.g., 2.5 cm for the WSR-88D) causes ψ_e to change by 180°, a large angular change, whereas the change $\delta\tau_s$ along τ_s is $\delta\tau_s = \lambda/2c$ (e.g., 1.67×10^{-10}s) a tiny fraction of τ_t. Thus scatterer motion is measured by changes in ψ_e. As a consequence, the pulsed-Doppler radar is an amplitude and phase sampling system (i.e., samples of As_{hh} and ψ_e at τ_s are obtained at T_s intervals). Range-time τ_s determines the range to the scatterer, and changes in ψ_e for echoes sampled at τ_s are measured from pulse-to-pulse along *sample-time* mT_s. Because of this sampling process, the sampled echo voltage is written in the following form,

$$V(\tau_s, mT_s) = I(\tau_s, mT_s) + jQ(\tau_s, mT_s) \tag{5}$$

where τ_s and mT_s determine the range $r = c\tau_s/2$ and sample-time, respectively. This sampled echo voltage can be represented as a vector on the *Argand diagram* (e.g., Figure 4b), with $I(\tau_s, mT_s)$ and $Q(\tau_s, mT_s)$ as the coordinates. The carrier-shifted vector has the amplitude $|V(\tau_s, mT_s)|$ and echo phase ψ_e (positive when measured ccw from the $I(\tau_s, mT_s)$ axis).

Echo Phase Shift

Because of (4), ψ_e changes with time as the scatterer's *r* changes at a rate corresponding to its v_r. This time rate-of-change of ψ_e is

$$\frac{\mathrm{d}\psi_{\mathrm{e}}}{\mathrm{d}t} = -\frac{4\pi}{\lambda}\frac{\mathrm{d}r}{\mathrm{d}t} = -\frac{4\pi}{\lambda}v_{\mathrm{r}} = 2\pi f_{\mathrm{d}} \quad . \tag{6a}$$

where,

$$f_{\mathrm{d}} = -\frac{2v_{\mathrm{r}}}{\lambda} \tag{6b}$$

is the Doppler frequency f_{d}. Although it is possible to calculate a radial velocity for each copolar signal, v_{r} is the same for each polarization.

As an example, the $I(\tau_{\mathrm{s}}, mT_s)$ and $Q(\tau_{\mathrm{s}}, mT_s)$ components from a 10-cm wavelength weather radar illuminating both stationary and moving scatterers are shown in Figure 4a as a function of τ_{s} for five successive transmitted pulses spaced T_s = 768x10^{-6} s. The echoes from the moving scatterer clearly exhibit a systematic change caused by v_{r}. Amplitudes of $I(\tau_{\mathrm{s}}, mT_s)$ and $Q(\tau_{\mathrm{s}}, mT_s)$ can change from a positive maximum to a negative maximum if the scatterer moves $\lambda / 4$ in T_{s}. As shown earlier, under this same condition, the echo's range-time τ_{s} changes less than 2x10^{-10} seconds, a shift too small to be detected in Figure 4a.

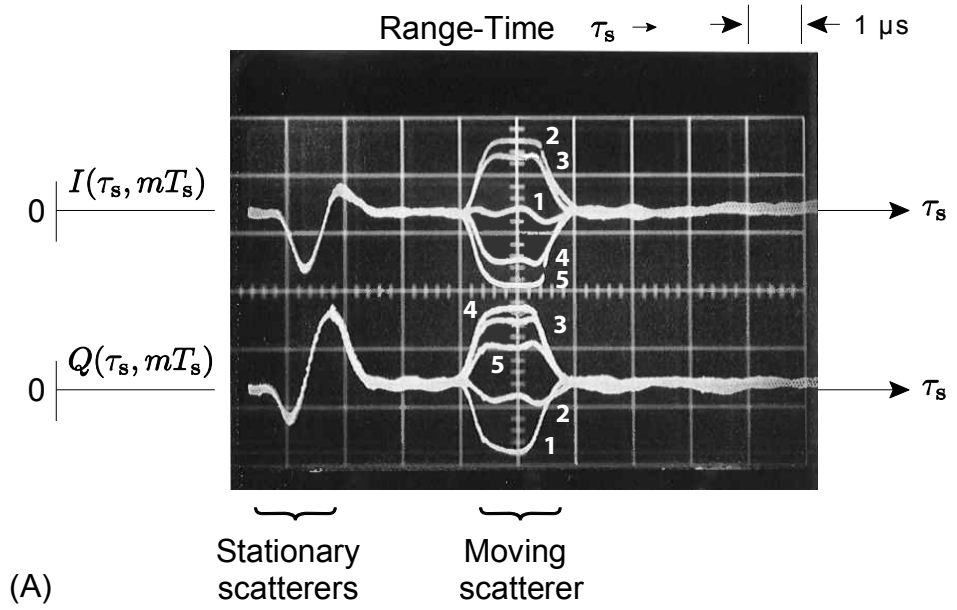

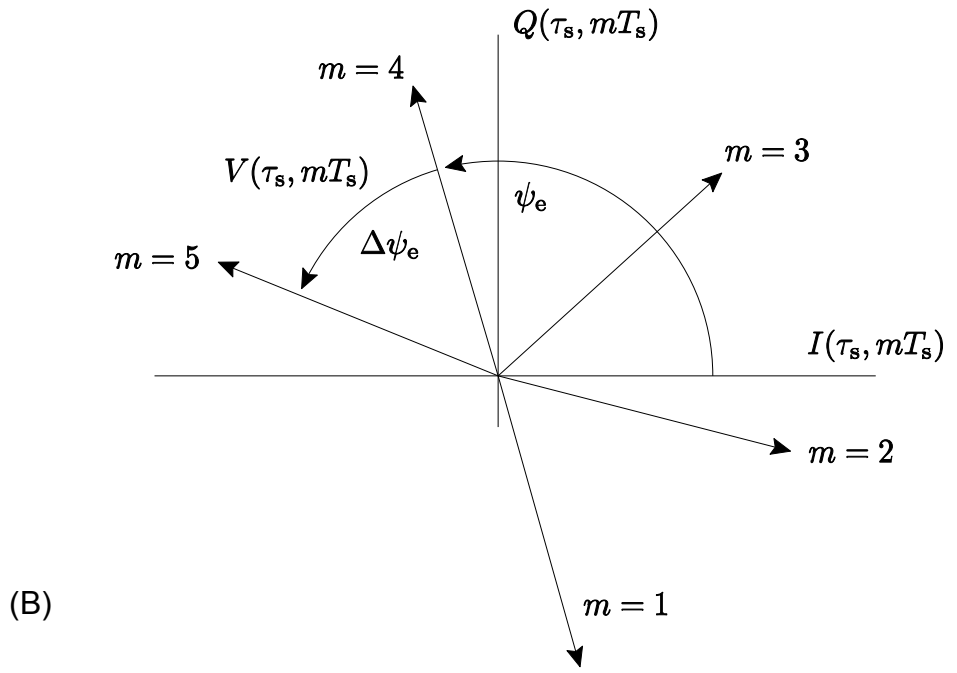

Figure 4 (a) In-phase and quadrature signals as a function of range-time for five successive intervals, T_s, superimposed to show the signals' relative change for stationary and moving scatterers. (b) An Argand diagram of the five samples in (a) at the five mT_s for the moving scatterer.

Let us now calculate f_d and v_r from the $I(\tau_s, mT_s)$ and $Q(\tau_s, mT_s)$ changes seen in Figure 4 for the moving scatterer. This scatterer's five samples are sketched on the Argand diagram in Figure 4b. We see that the echo vector samples rotate ccw about the origin, and by convention this corresponds to a positive Doppler shift. Because the echo phase change $\Delta\psi_e$ between pulse 1 and 2 is approximately 60^o during T_s,

$$f_d(\text{Hz}) = 60^o \times \frac{1\,\text{cycle}}{360^o} \times \frac{1}{T_s}$$

computes to be about +217 Hz. Using equation (6b), v_r computes to be about -10.9 m s^{-1}.

It should be mentioned that pulsed-Doppler radar inherently limits both the range and velocities that can be measured unambiguously. If the radar transmits a uniform periodic sequence of pulses, which is normally the case, it is not possible to determine which transmitted pulse produced which echo. Furthermore, the periodic transmitted pulse sequence also introduces velocity ambiguities. These problems are well illustrated in a like article in the first edition of this encyclopedia. There are several techniques to mitigate these ambiguities and the reader is referred to them for further reading (e.g., Bharadwaj and Chandrasekar 2007; Doviak and Zrnić 2006; Cho 2005; Sachidananda and Zrnić 2003; Torres, et al. 2004).

Volume Scattering

Up to this point, we have discussed scattering from a single scatterer – both stationary and moving. This theory is fundamentally the same as what underpins radar used to remotely detect aircraft, ships, missiles, planets, etc. Whereas most radars are designed to detect and characterize a countable number of discrete objects (i.e., aircraft, automobile, etc.), weather radars need to deal with countless numbers of non-distinctive scatterers which can be distributed over vast volumes of the atmosphere. The echo power from each atmospheric scatterer is very weak. For example, a one millimeter raindrop at r = 100 km returns a power less than 10^{-22} Watts. Although each scatterer's echo is weak and usually not detectable, the sum of echo powers from an extremely large number of scatterers within the radar beam can return a strong continuum of echoes as the transmitted pulse propagates through the field of scatterers.

Polarimetric Doppler weather radars are used to estimate and map the hydrometeors' fields of reflectivity factor (proportional to the number density and size of the hydrometeors), reflectivity weighted mean radial velocity, and polarimetric quantities; from these fields, radar meteorologists derive estimates of the fall rate and accumulation of precipitation, classify types of scatterers, and resolve storm hazards.

Other types of atmospheric radars such as wind profilers are designed to detect scatter from refractive index perturbations, caused by minute temperature and humidity variations, to measure wind in the lower atmosphere. Echoes from refractive index perturbations are called Bragg scatter (Doviak and Zrnic, 2006, Chapter 11). MST (Mesosphere, Stratosphere, and Troposphere) radars use large antennas (e.g., 100x100 m^2), long wavelengths (i.e., >> 1 m), and

high average power (e.g., few tens of kilowatts) to detect Bragg scatter from the weak refractive index perturbations in the upper atmosphere. Polarimetric Doppler weather radar can also detect Bragg scatter, but observations are limited to the troposphere, and conditions of strong refractive index perturbations.

After a delay (the time for the transmitted pulse to propagate to the near boundary of the volume of scatterers plus time for the first echoes to arrive at the radar), echoes are continuously received (Figure 5) during a time interval equal to twice the time it takes the microwave pulse to propagate across the volume of scatterers. Because one cannot resolve the echo from each scatterer, the radar's digital processors use gating circuits to sample the in-phase and quadrature signals at uniformly spaced time intervals along τ_s.

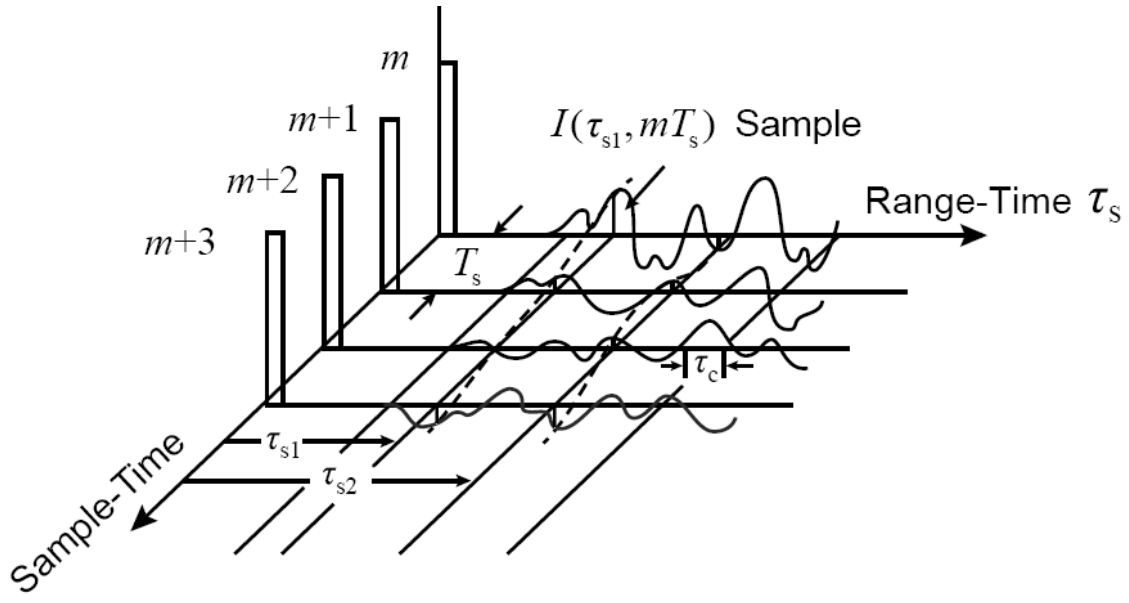

Figure 5 Idealized traces for $I(\tau_s, mT_s)$ of echoes from a distribution of scatterers. The solid line traces represent $I(\tau_s, mT_s)$ for the m^{th} T_s interval; dashed traces connect samples (i.e., the vertical line segments) at each τ_s.

Definition of the Resolution Volume

For each sample in range-time ($\tau_s = \tau_{s1}, \tau_{s2}, \tau_{s3,\ldots}$), there is a resolution volume V_6, at range $c\tau_s/2$, which is enclosed by the surface on which the angular and range weighting functions (determined by θ_1, τ_t and the receiver's bandwidth B_6) are 1/4 their peak value (i.e., 6 decibels below the peak); the surface has an angular width θ_1, and, for receiver bandwidth $B_6 > \tau_t^{-1}$, a range width about equal to $c\tau_t/2$. The scatterers within V_6 are those that significantly contribute to the sampled voltage at delay τ_s (Figure 5); those outside V_6 usually make a significantly smaller contribution. This process of volume integration is represented by the summation of the individual echo voltages in the following equation

$$V_{hh}(\tau_s, mT_s) = \sum_n A^{(n)} s_{hh}^{(n)} \exp\left\{ j\left[-\frac{4\pi r^{(n)}}{\lambda} - \frac{4\pi v_r^{(n)}}{\lambda} mT_s + \psi \right] \right\} \tag{7}$$

where the superscript (n) denotes the n^{th} scatterer. Gating circuits obtain digital samples of echoes from several hundred volumes along the beam. Examples of $I(\tau_s, mT_s)$ and $Q(\tau_s, mT_s)$ time series for echoes from scatterers in two independent V_6s is shown as a function of pulse number m in Figure 6. One of the volumes has echoes dominated by a stationary scatterer (e.g., a cell tower); this echo (called ground clutter because, for weather radar applications, it is unwanted and clutters signals from weather) produces a slowing varying voltage, variations mostly due to changes in scatterer illumination due to beam scan. However, swaying of foliage can also cause echo amplitude to slowly fluctuate. The more distant resolution volume contains moving hydrometeors, whose fast radial velocities cause rapid

variations of the echo voltage signal.

Spectral Analysis of the Echo Voltage

Temporal variations of the echo voltage in sample-time mT_s hold important Doppler information about the scatterers within the resolution volume. For each range-time τ_s, echo voltage samples from numerous pulses and for each polarization are compiled over the *dwell-time* (MT_s, the time to transmit all M pulses used in the analysis) chosen to investigate these variations. This so-called *spectral analysis* is usually accomplished using the discrete Fourier Transform of the echo voltage. The main product of the Fourier transform is the Power Spectral Density – also called the *Doppler Spectrum* in the weather radar community. The Doppler spectrum provides the reflectivity-weighted distribution of radial velocities of scatterers mostly within the resolution volume. Examples of Doppler spectra are provided in Figure 6 corresponding to the echo voltage samples previously discussed. Independent Doppler spectra can be obtained for both H and V polarization, providing the possibility of velocity-dependent polarimetric characterization.

For the ground clutter case shown in Figure 6, the Doppler spectrum shows a prominent peak at zero Doppler velocity because ground objects are mostly stationary. For weather, the peak of the Doppler spectrum estimates the weighted mean radial velocity of hydrometeors. More interestingly, the shape of the spectrum holds a wealth of information about inhomogeneities within the resolution volume, such as wind shear, multiple hydrometeor types, etc. This information can be quite useful when studying phenomena such has tornados, squall lines, microbursts, or any weather events with a high degree of structure.

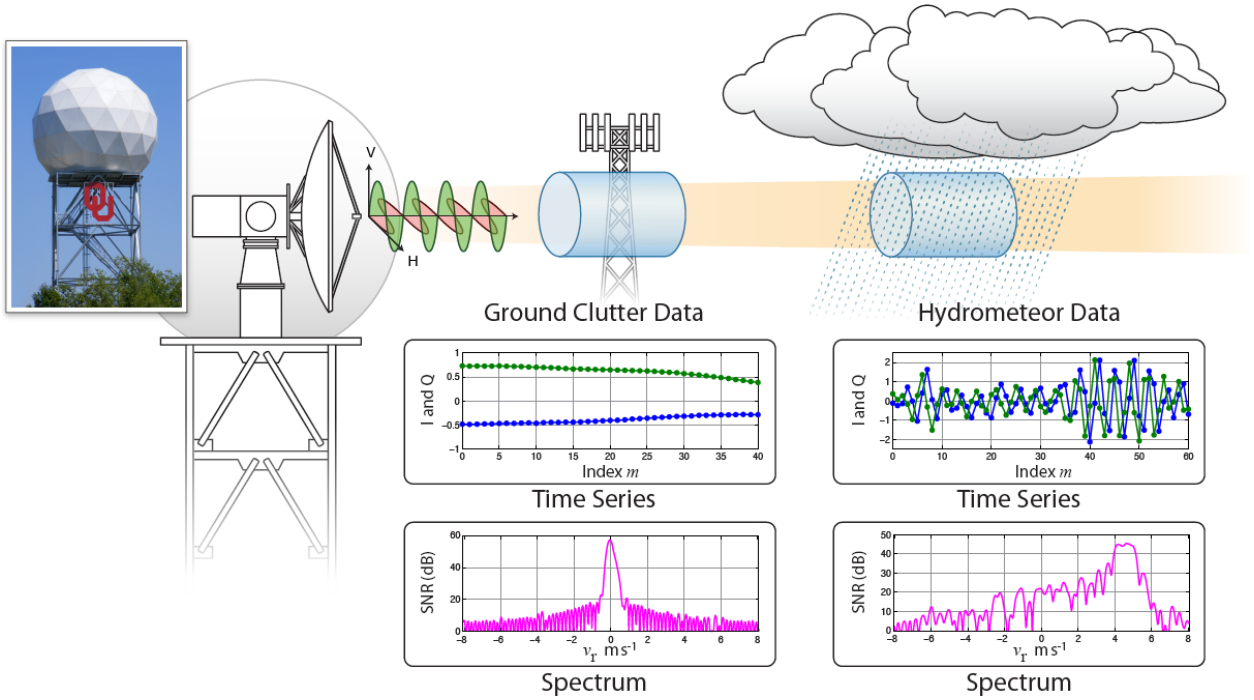

Figure 6 OU-PRIME weather radar showing idealized H and V waves propagating along the beam and two V_6s (i.e., quasi cylindrical resolution volumes), and time series traces $I\left(\tau_s, mT_s\right)$ and $Q\left(\tau_s, mT_s\right)$ of the echoes from the two V_6s for the H or V wave. Each trace is a sequence of echo samples (dots) spaced by mT_s. Also shown are the Doppler spectra of echo samples from the two V_6s for one polarization.

Spectral Moments and Polarimetric Products

Neither echo voltage nor Doppler spectra are typically recorded or displayed in real-time; rather, digitized samples from both H and V polarizations [i.e, $V_{hh}\left(\tau_s, mT_s\right)$ and $V_{vv}\left(\tau_s, mT_s\right)$] are collected over the desired dwell time and sent to the radar's signal processor. Due to the typically uniform distribution of reflectivity, turbulence, and mean wind shear within V_6, and the Gaussian shape of the beam's illumination, the Doppler spectrum often has a Gaussian shape.

In this case, only three parameters completely describe the spectrum – the zeroth, first, and second moments. The zeroth moment is the area under the Doppler spectrum and is proportional to the backscattered power for each polarized wave from a particular V_6. The first moment (i.e., the mean radial velocity $E[v_r]$) is the integral of the product of the Doppler velocities multiplied by the power spectrum normalized by the total spectral power, essentially providing the "center of mass" of the Doppler spectrum. The square root of the second moment of the Doppler spectrum is the spectrum width, σ_v, which is proportional to the spread of v_r within V_6; thus, it is a measure of turbulence and mean wind shear. It should be noted that separate moment estimates are obtained for both polarizations. The zeroth moments are quite useful, as will be described below. The radial velocity and spectrum width, however, do not have significant difference for H and V polarized waves.

Through careful calibration, the copolar backscattering matrix elements (s_{hh} and s_{vv}) can be derived from the complex echo signals with H and V polarizations. In turn, s_{hh} and s_{vv} are used to calculate important polarimetric products. The H and V reflectivity factors,

$$Z_h = \left(\frac{4\lambda^4}{\pi^4 |K_w|^2} \right) \langle |s_{hh}|^2 \rangle_{dV} \tag{9a}$$

$$Z_v = \left(\frac{4\lambda^4}{\pi^4 |K_w|^2} \right) \langle |s_{vv}|^2 \rangle_{dV} \tag{9b}$$

are proportional to the average backscattered cross-section per unit volume (e.g., $\langle |s_{hh}|^2 \rangle_{dV} = n(\vec{r}) \langle |s_{hh}|^2 \rangle$ where $n(\vec{r})$ is the density of scatterers), and K_w is the complex dielectric factor for water. The brackets in equation (9) indicate averaging over the ensemble of drop shapes, sizes,

and canting angles (alternatively averaging over mT_s); for spherical hydrometeors $\langle|s_{hh}|^2\rangle = \langle|s_{vv}|^2\rangle$. For larger drops, ice crystals, hail stones, etc., these polarimetric parameters can be quite different providing information about the shape (e.g., Figure 1) of the hydrometeors. To quantify this difference, the logarithm of the ratio of Z_h and Z_v is taken to produce

$$Z_{DR} \equiv 10\log_{10}\left(\frac{Z_h}{Z_v}\right) = 10\log_{10}\left(\frac{\langle|s_{hh}|^2\rangle}{\langle|s_{vv}|^2\rangle}\right) \tag{10}$$

Because s_{hh} is expected to be larger than s_{vv} for drops deformed by drag forces as shown in Figure 1, typical values of Z_{DR} for rain varies from 0 to +4 dB. For snow, ice crystals typically orient themselves horizontally and can have large aspect ratios, so Z_{DR} varies from +1 to +6 dB, depending on crystal habit.

Another important polarimetric product is the complex correlation coefficient

$$\rho_{hv}(nT_s) = \frac{\left\langle s_{vv}\left([m+n]T_s\right)s_{hh}^*\left(mT_s\right)\right\rangle}{\left\langle|s_{vv}\left(mT\right)|^2\right\rangle^{1/2}\left\langle|s_{hh}\left(mT\right)|^2\right\rangle^{1/2}} \tag{11}$$

a measure of the similarities of the time changes in s_{hh} and s_{vv}. The parameter that is most commonly displayed is $\rho_{hv}(0)$ the magnitude at zero lag (typically the magnitude symbols |x| are not displayed). $\rho_{hv}(0)$ is directly computed for STSR mode, but requires further processing and assumptions for the ATSR mode. Because $\rho_{hv}(0)$ is a normalized variable, it is independent of radar calibration. For spherical hydrometeors, $\rho_{hv}(0)$ should be close to unity but can be affected by the quality of the radar hardware (e.g., reflector, feed, etc.) and by the chosen polarimetric data acquisition mode. For more complex scatterer shapes (e.g., tornado debris), $\rho_{hv}(0)$ is reduced from unity – a fact that can be used for hydrometeor classification and tornado detection, for example.

As stated earlier, we have ignored propagation effects when describing polarimetric products, and have focused on only backscattering effects. Under certain conditions and depending on the radar wavelength, propagation effects can be important. The interested reader is referred to Doviak and Zrnić (2006) or Bringi and Chandrasekar (2001) for a more complete coverage of the topic.

Examples of Polarimetric Doppler Radar Data

Near the National Weather Center on its research campus, the University of Oklahoma (OU) operates a high-resolution, 5-cm wavelength polarimetric Doppler radar called OU-PRIME for *Polarimetric Radar for Innovations in Meteorology and Engineering* (Palmer et al. 2011, also see Figure 6 insert). The name was coined to emphasize the fact that the radar is used for collaborative research and education in both science and engineering.

On May 10, 2010, a tornado outbreak occurred in Oklahoma producing numerous strong tornadoes with the largest two having EF-4 ratings. Unfortunately, three deaths were reported along with significant property damage. Several of the more powerful tornadoes formed very near OU-PRIME (less than 1 km) providing polarimetric radar data of unprecedented resolution and quality. An example of the data is provided in Figure 7 in what is called a *plan position indictor* (PPI) display, where the radar beam is kept at a constant elevation angle while rotating in azimuth. For the May 10 case, the four major products of a polarimetric radar are Z_{h}, v_{r}, Z_{DR}, $\rho_{\mathrm{hv}}(0)$. The most prominent feature of the reflectivity data (panel a) is the spiral of high reflectivity, the so-called "hook echo" often associated with a tornado. The tornado itself is likely located at the tip of the "hook" where there is a small blob of high reflectivity (likely due to

tornadic debris) with an "eye" of lower reflectivity. The radial velocity field (panel b) shows the well-known velocity couplet of out- ($+v_r$) and in-bound ($-v_r$) radial velocities (red and green, respectively) caused by the rotation of the tornado. Z_{DR} data (panel c) exhibit very high values (red area, the so-called "Z_{DR} Arc"; Kumjain and Ryzhkov 2008), indicative of large drops near the storm's eastern edge. The correlation coefficient field $\rho_{hv}(0)$, shown in panel (d), illustrates the classic debris signature of low $\rho_{hv}(0)$ values near 0.6 at the tip of the hook echo (Ryzhkov et al. 2002).

Through the combination of the various signatures of the polarimetric data, it is possible to greatly improve the performance of tornado detection algorithms and hydrometeor classification techniques, for example. After extensive research on polarimetric radar has been conducted, the operational WSR-88D radars are now being upgraded with polarimetric capability. With this advent, new scientific applications are sure to be developed over the coming years.

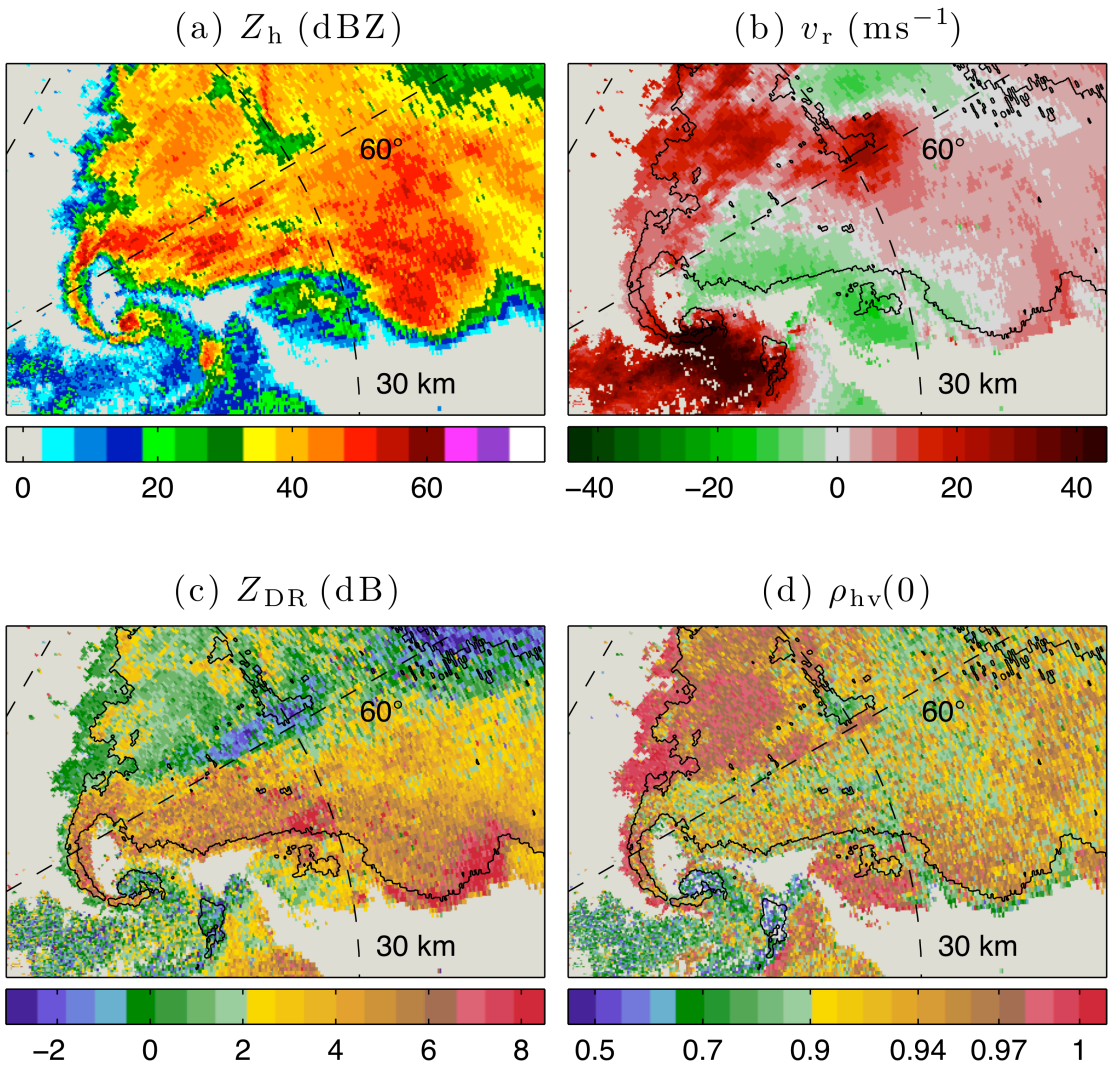

Figure 7 OU-PRIME measurements of (a) reflectivity factor Z_h, (b) radial velocity v_r, (c) differential reflectivity Z_{DR}, and (d) correlation coefficient $\rho_{hv}(0)$ at 1.0° elevation angle from the sector scan started at 2245 UTC on May 10, 2010. The radar is located off the lower-left of the figure and a 30-km range ring provided for orientation. On panels b, c, and d, a 35-dBz contour line is provided to show features of the various parameters relative to the Z_h field.

Future Weather Radar – Phased Array Antennas

The history of weather radar is replete with examples of significant steps forward in technology because of developments for military applications. Prime examples include advances in transmitter technology (e.g., magnetron) and Doppler capabilities. The future of weather radar will very likely show a continuation of this trend.

One technology, which has been used in military radar for decades and is just now being tested in the weather radar community, is electronic beam scanning using *phased array antennas* (Weber et al. 2007, Zrnić et al. 2007). As previously described, conventional weather radars provide complete coverage of storms by mechanically rotating a parabolic reflector antenna. Since the antenna is a very large and heavy structure, it is typically rotated continuously in azimuth and stepped in elevation without rapid starts or stops of the antenna. By doing so, the mechanical stresses on the gears and motors are minimized, prolonging the life of the entire system and reducing maintenance costs. Phased array antennas operate in a completely different way without any mechanical motion.

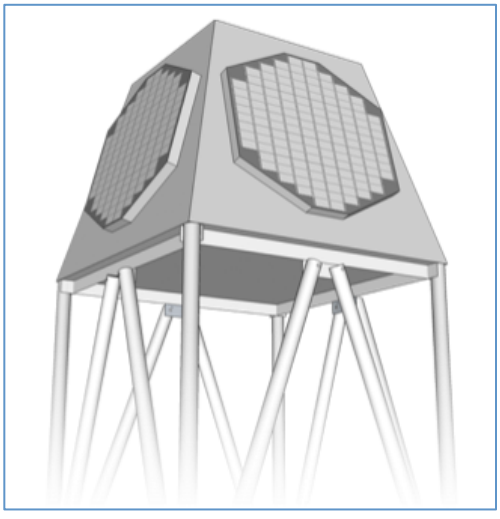

Figure 8 Artist's depiction of a four-panel phased array weather radar (PAR).

Each face of a phased array antenna is made up of thousands of individual radiating elements spread over the quasi-circular aperture of the array, which is usually a planar surface (Figure 8). The beam formed by each face azimuthally scans $\pm 45^{o}$ about a vertical plane containing the broadside direction (i.e., the line perpendicular to the array surface). To observe a full 360-degree coverage, four phased array panels are needed. Each element of the array is a transmitter and receiver and each has a commanded amplitude and phase; the amplitude distribution across the aperture controls the beamwidth and sidelobe levels, and the phase distribution controls the direction of the beam. If the phase is uniform across the array, the surface of constant phase of the radiated field is perpendicular to the broadside direction and the beam is along the broadside direction. If the phases of the array elements are adjusted so that the surface of constant phase is tilted relative to the array face, the beam will be pointed in a direction perpendicular to the constant phase surface.

These commanded phase shifts can be generated and changed electronically from pulse to pulse allowing extremely rapid beam steering with no mechanical motion of the antenna. Furthermore, the beam agility provided by electronic steering allows adaptive scanning so the beam need only scan stormy regions of interest rather than having equal dwell times on regions of clear skies (Heinselman and Torres 2011). Such a capability for weather PAR exists with the National Weather Radar Testbed (NWRT), which has a phased array antenna on loan from the US Navy, and a WSR-88D transmitter, and is located on the campus of the University of Oklahoma.

Because of this capability, phased array weather radars hold promise for improved observations of rapidly evolving severe weather phenomena. Furthermore, a beam from the same panel but at a different frequency can be pointed in different directions allowing multi-mission applications (e.g., a single antenna could be used to both observe weather and track aircraft). Also PAR has the capability to operate with more than one beam for each mission (i.e., one beam for each array panel), thus increasing the update rate of data to improve forecasts and warnings (Stensurd et al. 2009).

As with any new technology, significant challenges exist, such as combining radar polarimetry with phased array antennas. Most military radars use single polarized waves whereas the USA National Weather Service has accepted radar with dual polarization capability to better forecast weather and issue warnings. Thus, one such challenge is to develop a Polarimetric Phased Array Radar (PPAR) that has better capability than polarimetric weather radars using parabolic reflector antennas. The PPAR (Figure 8) has beamwidths and polarimetric wave properties that depend on the direction of the beam and calibration is much more complicated than needed for the existing weather radars (Zhang et al., 2009) The adaptation of dual polarimetry to PPAR opens research opportunities to overcome some of these complexities.

A solution under study is the use of a Cylindrical Polarimetric Phased Array Radar (CPPAR, Figure 9; Zhang et al., 2011). With this phase array antenna the phases of the elements are adjusted to produce a plane surface of constant phase so that the beam width and polarimetric properties are the same independent of azimuth angle. By commutating the amplitude and phase commands around the periphery of the cylinder, the beam scans in azimuth without changes in beamwidth or polarimetric properties. Nevertheless, there are changes in these properties when the beam is elevated, but for weather applications the most important

beam directions are those close to the ground and perpendicular to the axis of the cylinder. It remains to be shown that PPAR or CPPAR can exploit their rapid scanning capability while providing weather data with the same quality presently achieved with reflector antennas. This notwithstanding, it is possible that over the next decades phased array weather radar will be fully developed and used for operational networks around the world.

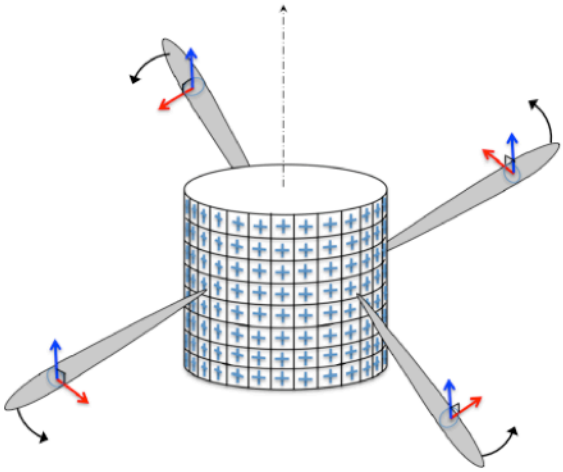

Figure 9 Artist's depiction of cylindrical polarimetric phased array weather radar with pairs of dipoles for each array element antenna (from Zhang et al., 2011). Shown is red (blue) is the H (V) polarized wave and four simultaneous beams are assumed. Beams at other frequencies can be added and steered independently for use in other missions.

Acknowledgements

The authors express their appreciation to Dr. Boon Leng Cheong, of the Atmospheric Radar Research Center, University of Oklahoma, who provided the figures.

Glossary

A echo amplitude

ATSR alternate transmit simultaneous receive

B_6 receiver bandwidth

De equivalent diameter of a rain drop

E_h, E_v electric field components polarized horizontally, vertically

c speed of light

$E[x]$ mean or expected value of x

f_t transmitted frequency

f_d Doppler frequency

$I(r,t)$ real part of $V(r,t)$

j $\sqrt{-1}$, Imaginary unit

K_w the complex dielectric factor for water

m integer index

$n(\vec{r})$ scatterer density

P_{av} average power transmitted

P_t peak power transmitted

PAR phased array radar

PPAR polarimetric phased array radar

NWRT National Weather Radar Testbed

$Q(r,t)$ imaginary part of $V(r,t)$

r range

s_{hv} complex backscattering matrix element

STALO stabilized local oscillator

STSR simultaneous transmit simultaneous receive

t time

T_s pulse repetition time (sampling time)

$U(x)$ $U = 1$ if $0 < x < \tau$; otherwise $U = 0$

$V(r,t)$ echo voltage

V_6 resolution volume

v_r radial velocity

WSR weather surveillance radar

Z_h, Z_v the reflectivity factor measured with H, V polarized waves

Z_{DR} differential reflectivity factor

$\dot{\cdot}\dot{\cdot}_0$ beam azimuth

$\dot{\cdot}\dot{\cdot}$ beam azimuth relative to north

θ_e beam elevation angle

θ_0 zenith angle

θ_1 one-way beamwidth at the half-power level

λ wavelength

σ_v spectrum width

σ_τ correlation-time along mT_s

τ_c correlation-time along τ_s

τ_s range-time

τ_t transmitted pulse width

ψ sum of phase shifts within the radar and the scatterer

ψ_e echo phase

Further Reading

Bharadwaj, N and Chandrasekar V (2007) Phase Coding for Range Ambiguity Mitigation in Dual-Polarized Doppler Weather Radars. *Journal of Atmospheric and Oceanic Technology* 24(8): 1351-1363.

Bringi, VN and Chandrasekar V (2001) Polarimetric Doppler Weather Radar: Principles and Applications, Cambridge Press.

Chandrasekar V and Bharadwaj N (2009) Orthogonal Channel Coding for Simultaneous Co- and Cross-Polarization Measurements, *Journal of Atmospheric and Oceanic Technology* 26: 45-56.

Cho JYN (2005) Multi-PRI Signal Processing for the Terminal Doppler Weather Radar. Part II: Range–Velocity Ambiguity Mitigation. *Journal of Atmospheric and Oceanic Technology*. 22(10): 1507-1519.

Doviak RJ and Zrnić DS (2006) *Doppler radar and weather observations*, 2nd Edn. Dover Publications.

Doviak RJ, Bringi V, Ryzhkov A, Zahrai A, and Zrnić DS (2000) Considerations for polarimetric upgrades to operational WSR-88D radars. *J. Atmos. Oceanic Technol.*, 17, 257 – 278.

Heinselman P and Torres S (2011) High-temporal-resolution capabilities of the National Weather Radar Testbed Phased-Array Radar. *J. Appl. Meteor. Climatol*., 68, xxx-xxx. DOI:10.1175/2010JAMC2588.1.

Kumjian MR and Ryzhkov A (2008) Polarimetric signatures in supercell thunderstorms. *J. Appl. Meteor. Climatol.*, 48, 1940 – 1961.

Palmer RD, Bodine D, Kumjian M, Cheong B, Zhang G, Cao Q, Bluestein HB, Ryzhkov A, Yu T, Wang Y (2011) Observations of the 10 May 2010 Tornado Outbreak Using OU-PRIME: Potential for New Science With High-Resolution Polarimetric Radar, Bulletin of the American Meteorological Society.

Pruppacher HR and Beard KV (1970) A wind tunnel investigation of the internal circulations and shape of water drops failing at terminal velocity in air, Quart. J. Roy. Meteorol. Soc., 96, 247-256

Ryzhkov A, Burgess D, Zrnić D, Smith T, and Giangrande S (2002) Polarimetric analysis of a 3 May 1999 tornado. Preprints, *22nd Conf. on Severe Local Storms,* Hyannis, MA, Amer. Meteor. Soc., 14.2. [Available online at http://ams.confex.com/ams/pdfpapers/47348.pdf.]

Sachidananda M and Zrnić DS (2003) Unambiguous Range Extension by Overlay Resolution in Staggered PRT Technique. *Journal of Atmospheric and Oceanic Technology*. 20 (5) 673-684.

Stensrud DJ, Xue M, Wicker JL, Kelleher KE, Foster MP, Schaefer JT, Schneider RS, Benjamin SG, Weygandt SS, Ferree JT, and Tuell JP (2009) Convective-Scale Warn-On-Forecast System, Bulletin of the American Meteorological Society, Volume 90, Issue 10, pp. 1487-1499.

Torres SM, Dubel YF, Zrnić D (2004) Design, Implementation, and Demonstration of a Staggered PRT Algorithm for the WSR-88D. *Journal of Atmospheric and Oceanic* Technology. 21(9): 1389-1399.

Weber ME, Cho JYN, Herd JS, Flavin JM, Benner WE, Torok GS (2007) The Next-Generation Multimission U.S. Surveillance Radar Network, Bulletin of the American Meteorological Society, Volume 88, Issue 11, pp. 1739-1751.

Zhang G, Doviak RJ, Zrnić DS, Crain J, Stainman D, Al-Rashid Y (2009) Phased array radar polarimetry for weather sensing: A theoretical formulation for bias correction. *IEEE Geosci. Rem. Sens.*, 47, 3679-3689.

Zhang G, Doviak RJ, Zrnić DS, Palmer, RD, Lei L, and Al-Rashid Y (2011) Polarimetric Phased Array Radar for Weather Measurement: A Planar or Cylindrical Configuration?, *Journal of Atmospheric and Oceanic Technology*, in press.

Zrnić D, Kimpel JF, Forsyth DE, Shapiro A, Crain G, Ferek R, Heimmer J, Benner W, McNellis

TJ, Vogt RJ (2007) Agile-Beam Phased Array Radar for Weather Observations, Bulletin of the American Meteorological Society, Volume 88, Issue 11, pp. 1753-1766.